Thin Films of a Main-Chain Columnar Liquid Crystal: Studies of Structure, Phase Transitions, and Alignment

Matthieu Defaux,[†] Loïc Vidal,[†] Martin Möller,[‡] Raluca I. Gearba,[§] Elaine DiMasi,[||] and Dimitri A. Ivanov*,[†]

Institut de Sciences des Matériaux de Mulhouse-IS2M, CNRS LRC 7228, Jean Starcky, 15, F-68057 Mulhouse, France; Deutsches Wollforschungsinstitut an der RWTH Aachen e.V., Pauwelsstr. 8, 52074 Aachen, Germany; Center for Functional Nanomaterials, Brookhaven National Laboratory, P.O. Box 5000, Upton, New York 11973; and National Synchrotron Light Source, Brookhaven National Laboratory, P.O. Box 5000, Upton, New York 11973

Received November 27, 2008; Revised Manuscript Received March 22, 2009

ABSTRACT: The structure of thin films of poly(di-*n*-propylsiloxane), PDPS, was studied with a combination of optical and atomic force microscopy, electron diffraction, and grazing incidence X-ray diffraction. Two different morphological features are observed in the mesomorphic films. The lamellar ribbons are composed of the chains oriented parallel to the plane of the substrate in which the reciprocal space **10** vector is vertical. The other feature with a circular symmetry, the cylindrite, contains the chains parallel to the substrate normal. The cylindrites and needles are essentially the same mesomorphic lamellae that develop differently under the conditions of confinement. The crystallization of PDPS films does not change the gross morphological features developed during the mesophase formation and mainly proceeds via epitaxial growth of the α-crystal on the parent mesophase. Spontaneous alignment of the mesomorphic PDPS films on the PTFE-rubbed substrates allows fabricating highly crystalline inorganic polymer surfaces oriented on the scale of centimeters.

1. Introduction

In the past years, important efforts were devoted to fabrication of materials organized on multiple scales by self-assembly. Controlling the structure of thin films and surfaces at spatial scales ranging from angstroms to centimeters was found crucial for both conventional applications such as membranes[1] and sensors[2] and less conventional ones such as light-emitting diodes,[3] photovoltaic cells,[4] and field effect transistors.[5] For example, for films of poly(3-hexylthiophene) a change in the lamellar orientation with respect to the substrate can change the charge carrier mobility by 2 orders of magnitude.[6] However, the control of the morphology and alignment of crystalline films is not simple due to a high free energy change associated with the phase transition. For example, many studies address spatially confined crystallization for the case of diblock copolymers having one crystallizable block. In this case, the crystallization could be templated by the initial microphase-separated structure such as the nanometer-sized spheres, cylinders, or lamellae. Nevertheless, the literature results show that crystallization can easily disrupt the initial matrix,[7] giving rise to the so-called "breakout crystallization". Apart from the spatial confinement, the control of the crystal quality and orientation are even more difficult to achieve by this method. An extensive meticulous study of the various critical factors for the spatial control of the crystallization process and crystal alignment for the case of PEO-*b*-PS diblock copolymers has been performed by SZD Cheng and co-workers (cf. for example refs 8 and 9). Generally, an important pitfall of the block copolymer-based approach consists in the entangled and rather disordered state of polymer segments prior to crystallization; i.e., the degree of confinement is often insufficient to affect the chain orientation and guide the crystallization on the molecular scale.

The liquid crystalline (LC) state of macromolecules can allow for the required chain ordering and alignment before the structure is arrested in the course of crystallization. The conventional side-chain LC polymers are known to form nematic, smectic, and cholesteric LC phases due to ordering of the mesogenic moieties attached to the backbone.[10] However, the organization of the side chains in a LC phase does not necessarily imply anisotropic packing of the backbones.[11] In contrast, the occurrence of the LC phases in the main-chain LC polymers, such as the ones built up from cylinder-shaped monomers, is due to packing of the backbones, owing to their form anisotropy. More recently, hexagonal columnar mesophases formed by a variety of polymers were reviewed and classified in a thorough work of Ungar.[12] The physical properties of columnar phases such as the anisotropic viscosity and high chain mobility can make them promising in view of fabrication of highly crystalline defect-free polymer surfaces. Some of these materials can be processed from solution, which is very interesting from the technological viewpoint. In addition, the LC state of the material can allow for a facile processing and aligning of the film. In this case, the hexagonal LC phase already imposes a natural spatial confinement on polymer chains: each of them becomes squeezed within a cylinder of about 1 nm in diameter. To control the thin film preparation, it is thus important to first understand the film microstructure and phase transitions mechanisms. However, such information on thin mesomorphic films is very scarce in the literature. The results reported in the past focus mainly on side-chain liquid crystalline copolymers with semifluorinated chains.[13,14]

Previously, extensive studies have been performed on the mechanisms of the lamellar growth and thickening of polyethylene in the hexagonal phase formed at elevated pressures.[15] However, detailed morphological studies under these conditions are not easy. For example, sample observations with electron microscopy can be performed only post mortem, i.e., at ambient pressure, when the sample structure converts back to the orthorhombic phase stable under normal conditions. To be able to assess the mesophase structure formation in situ, another

* To whom correspondence should be addressed: Tel +33 3 89 60 87 00; fax +33 89 60 87 99; e-mail dimitri.ivanov@uha.fr.
[†] CNRS LRC 7228.
[‡] Deutsches Wollforschungsinstitut an der RWTH Aachen e.V.
[§] Center for Functional Nanomaterials, Brookhaven National Laboratory.
[||] National Synchrotron Light Source, Brookhaven National Laboratory.

10.1021/ma802666a CCC: $40.75
Published on Web 04/21/2009

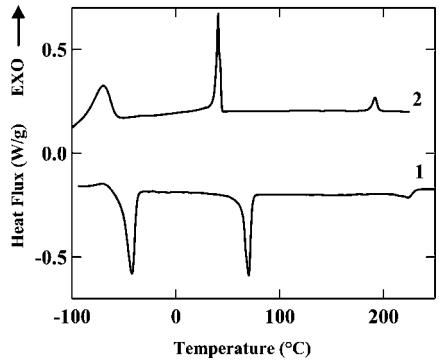

Figure 1. DSC curves recorded during heating (1) and cooling (2) at 10 °C/min of a PDPS sample with $M_w = 548\,000$.

model columnar liquid crystal has been chosen in this work, namely poly(di-*n*-propylsiloxane) (PDPS).

Symmetrically substituted poly(di-*n*-alkylsiloxanes) containing from two to six carbons per side chain are known to form columnar mesophases, without having any mesogenic groups in their structure.[16−20] The temperature window of the mesophase stability is strongly dependent on both the molecular weight of the main chain and length of the side chain.[17−24] The relationship between the isotropization temperature and reciprocal molecular weight was reported to be linear,[17−20] suggesting that the chains have a largely extended conformation in the mesophase. This was also confirmed in small-angle neutron scattering experiments that showed the existence of partly stretched chains in the mesophase.[25] With three carbons per side chain, PDPS forms a hexagonal mesophase stable over more than 130 °C. Apart from the mesophase, it forms two crystalline polymorphs.[17−19,23,24,26−28] The low-temperature crystalline phase β is characterized by a monoclinic unit cell with the following lattice parameters $a = 20.60$ Å, $b = 19.22$ Å, $c = 4.95$ Å, and $\gamma = 93.1°$. The high-temperature crystalline phase α has a pseudotetragonal unit cell with $a, b = 19.15$ Å and $c = 5.00$ Å and a monoclinic *C*2/*c* (No. 15) group symmetry.[28] In bulk, the crystallization of PDPS on cooling is so fast that amorphous samples cannot be obtained even during a temperature quench.[17,20,23,27,29] The formation of the mesophase during cooling is also very fast, suggesting that crystallization always proceeds through the mesomorphic state. The formation of the mesophase can be overcome when crystallization occurs from a dilute solution in the form of single crystals.[30] The bulk crystallinity of PDPS, as measured by DSC, X-ray diffraction, and solid-state NMR, typically exceeds 90%, which can be accounted for by the existence of a preordered mesomorphic state of the chains prior to crystallization.[17,20,28]

In this work, the stages of the structure formation in thin PDPS films such as the isotropic−liquid crystalline transition and mesophase-assisted crystallization were studied using different microscopy techniques as well as selected-area electron diffraction (SAED) and grazing incidence X-ray diffraction (GIXD).

2. Materials and Methods

2.1. Materials. Two PDPS samples with molecular weights of 548 000 and 269 000 g mol^{-1} and polydispersities of 2.02 and 2.06, respectively, were synthesized by anionic ring-opening polymerization of hexapropylcyclotrisiloxane as described elsewhere.[21,22,24] Unless specified, the results given below correspond to the PDPS sample with molecular weight of 548 000 g mol^{-1}. DSC measurements were conducted during cooling and heating ramps from −100 to 250 at 10 °C min^{-1}. Figure 1 shows DSC traces for the case of the higher molecular weight PDPS sample. Three reversible endothermic transitions are observed for both samples. The first low-temperature transition corresponds to the polymorphic crystal−crystal transition between the low-temperature β-phase and high-temperature α-phase, while the second transition is assigned to the melting of the α-phase in a hexagonal columnar mesophase. The temperature stability of the mesophase spans over ∼150 °C, with the sample isotropization occurring at 225 °C. The comparison between heating and cooling traces shows hysteresis effects, typical of the first-order transitions. The characteristic phase transition parameters are summarized in Table 1.

PDPS films with submicron thickness were prepared by spin-coating polymer solutions in toluene on a Si/SiO_2 substrates and on PTFE-rubbed surfaces. The work reported here was carried out mainly on PDPS films of ∼400 nm thickness. For the SAED experiments the films of about 100 nm thickness were used.

The PTFE rubbing was performed using a home-built machine operated at 300 °C at the deposition rate of 0.63 mm s^{-1}. During rubbing, a thin PTFE film is deposited on the substrate, in which the chains are aligned in the rubbing direction.[31]

2.2. Methods. *DSC measurements* were performed with a Mettler Toledo 822^e heat flux instrument coupled to a cryo-unit cooled with liquid nitrogen. The calorimeter was calibrated using melting enthalpies and temperatures of Zn and In.

Optical microscopy (OM) observations were carried out using an Olympus BX51 microscope equipped with a digital color camera Olympus DP70. Differential interference contrast accessory was used to study the morphology of thin supported films. The different phase transitions were observed using a Mettler-Toledo FP82 heating stage equipped with a FP90 central processor.

GIXD experiments were conducted at Beamline X6B, National Synchrotron Light Source, Brookhaven National Laboratory, using X-ray energy of 15.8 keV. Samples were contained in a chamber with Kapton windows equipped with a computer-controlled heating stage Instec HCS402 with liquid nitrogen cooling. The focused beam of 0.25 mm vertical × 0.5 mm horizontal was incident on the sample film at an angle θ_{inc} of 0.2°. The diffraction pattern was collected using a CCD detector from Princeton Instruments, having a 120 mm × 120 mm image area (2084 × 2084 pixels). Raw images were corrected for dark count, flat field, and spatial distortion using calibration frames obtained with a ^{55}Fe source, using the methods described in ref 32 and a brass plate machined with 1 mm holes on a square grid of 2.54 mm pitch. Detector-to-sample distance, typically 240 mm, was calibrated using measurements of Ag behenate powder.

Atomic force microscopy (AFM) experiments were carried out with a Nanoscope IV Multimode AFM (Veeco Metrology Group) in Tapping mode, which is most suitable for soft materials imaging. Tapping mode Si probes from Nanosensors were used (PPP-NCL, resonant frequency 172−191 kHz, spring constant 33−47 N/m). Previous works on PDES and mesomorphic polymers have shown the interest of tapping mode to reveal morphological details in crystalline and liquid crystalline regions.[28,30,33,34] The quantitative AFM image treatment was performed using the one-dimensional SAXS-type correlation and interface distribution functions as described previously.[35,36] Briefly, in the first step the images were converted to the binary form using home-built object recognition routines written in Igor Pro (Wavemetrics Ltd.). Further on, the

Table 1. Thermal Behavior of PDPS Samples[a]

N	$M_w \times 10^{-3}$ [g/mol]	T_{cr-cr}[b] [°C]	ΔH_{cr-cr} [J/g]	T_m[b] [°C]	ΔH_m [J/g]	T_i[b] [°C]	ΔH_i [J/g]
I	269	−46.4	32.9	68.1	21.9	225.0	4.0
II	548	−42.5	24.5	70.1	19.0	224.4	3.3

[a] Key: N, sample number; M_w, molecular weight; T_{cr-cr}, low-temperature polymorphic transition; T_m, melting temperature; T_i, isotropization point; ΔH, enthalpy variation. [b] The temperatures correspond to heating ramps at 10 °C/min.

two-dimensional power spectral density function ($P_2(\mathbf{s})$) was computed from AFM images ($u(\mathbf{r})$) up to the critical, or Nyquist, frequency depending upon the experimental sampling interval as

$$P_2(\mathbf{s}) \equiv \frac{1}{A}\left| \int_A u(\mathbf{r})W(\mathbf{r}) \exp(2\pi i \mathbf{s}\cdot\mathbf{r})\, \mathrm{d}^2\mathbf{r}\right|^2 \quad (1)$$

where A denotes the image area, $W(\mathbf{r})$ the window function,[37] and $\mathbf{s}$ the 2D reciprocal space vector. The $P_2(\mathbf{s})$ function was then transformed into the one-dimensional PSD ($P_1(s)$), where s stands for the norm of $\mathbf{s}$, according to

$$P_1(s) = (2\pi s)^{-1} \int P_2(\mathbf{s}')\delta(|\mathbf{s}'| - s)\, \mathrm{d}\mathbf{s}' \quad (2)$$

and finally, the one-dimensional SAXS-type correlation function[38] was computed as the real part of the Fourier transform of $P_1(s)$:

$$\gamma(l) \cong \mathrm{Re}\{2\pi \int_0^\infty P_1(s)s \exp(2\pi i s l) \exp(4\pi^2\sigma^2 s^2)\, \mathrm{d}s\} \quad (3)$$

where the $P_1(s)$ function was preliminarily corrected for the presence of the sigmoidal gradient crystal/amorphous transition layers having thickness σ.[39] Since the absolute values of the power spectral density function of AFM images do not have any particular physical meaning (contrary to the absolute intensity measurements in SAXS), the function $\gamma(l)$ was normalized to 1 at the origin. The interface distribution function $\gamma''(l)$ defined here as a convolution of the first derivatives of the profile measured across the lamellar stack:

$$\gamma''(l) = \frac{\mathrm{d}\rho(l)}{\mathrm{d}l} * \frac{\mathrm{d}\rho(-l)}{\mathrm{d}l} \quad (4)$$

was calculated as a second derivative of $\gamma(l)$:

$$\gamma''(l) = \frac{\mathrm{d}^2\gamma(l)}{\mathrm{d}l^2} \quad (5)$$

The $\gamma''(l)$ is often used to calculate the morphological parameters of the semicrystalline structure such as the most probable crystal thickness (L_c) since $\gamma''(l)$ can be expanded in a series of different interface distribution functions with alternating signs:[40]

$$\gamma''(l) \cong h_c(l) + h_a(l) - 2h_{ac}(l) + \ldots \quad (6)$$

The first three distribution functions in (6) correspond to the crystal and amorphous thickness, $h_c(l)$ and $h_a(l)$, respectively, whereas the third one is the intercrystalline distance distribution, $h_{ac}(l)$, which is commonly termed the "long period".

Selected-area electron diffraction (SAED) experiments were carried out with a Philips CM200 transmission electron microscope operated at 200 kV. Calibration of the electron diffraction patterns has been performed using gold.

3. Results and Discussion

3.1. Morphology of the As-Spun-Cast PDPS Films. The structure formation in spun-cast PDPS films usually completes within several seconds after the film preparation at room temperature. It results in a rather featureless crystalline morphology, as observed with OM (cf. Figure 2, top). AFM micrographs show that, on a smaller scale, the films are composed of slightly elongated objects with dimensions ranging from 80 to 400 nm having random orientation (Figure 2, middle). The thermal behavior of this structure was explored by step-annealing the films to a progressively higher temperature. It was found that the initial morphology remained largely unaffected by annealing at temperatures up to the isotropization point of PDPS (ca. 225 °C). Therefore, the chain mobility in the columnar mesophase of PDPS is insufficient to transfer the system to a state with a lower free energy.

The SAED recorded from one of such regions is given in Figure 2 (bottom). The pattern shows the presence of locally oriented crystalline domains characterized by arced reflections. The observed diffraction peaks of the pseudotetragonal unit cell

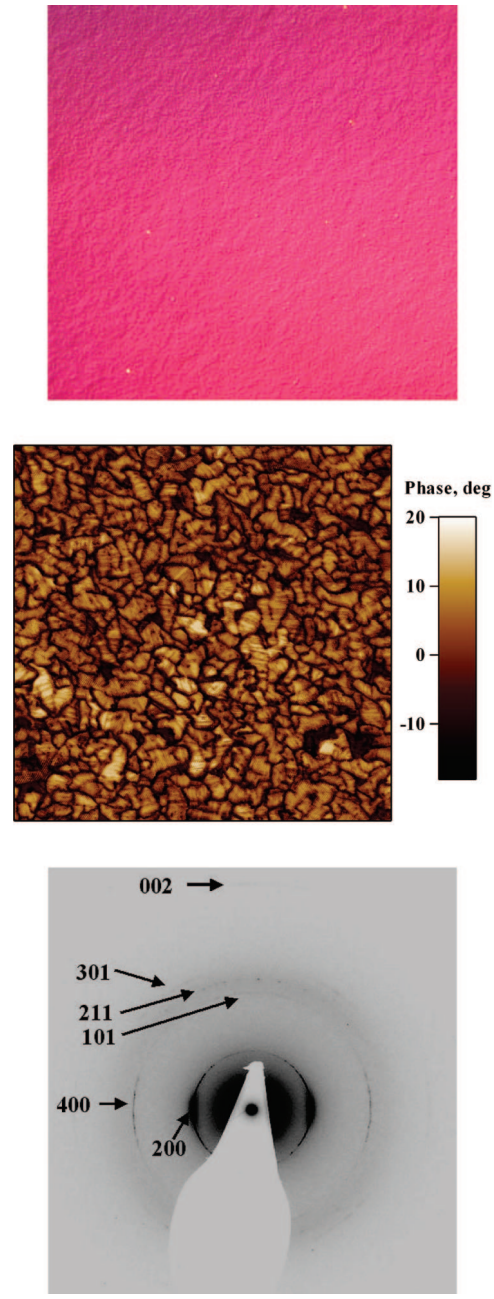

Figure 2. Optical (top) and AFM Tapping Mode phase (middle) micrographs of a PDPS film spun-cast on a Si/SiO_2 substrate. Scale: 440 × 330 μm^2 (top), 1.5 × 1.5 μm^2 (middle). Bottom: SAED pattern showing local orientation in the film. The pattern corresponds to [100]/[010] diffraction zone.

of the α-phase of PDPS[28] belong to the [010]/[100] diffraction zones (cf. Table 2), which are indistinguishable for this crystalline phase. The agreement between the experimental and calculated spacings is found to be very good. Despite pronounced arcing, the observed diffraction patterns are not of the fiber type. Thus, for example the strong equatorial 220 or 420 peaks are absent from the patterns, which would be impossible for a sample with uniaxial symmetry. The 211 peak, extraneous to both diffraction zones, is observed due to its proximity to the corresponding Ewald sphere.

GIXD experiments were performed on the films spun-cast on bare Si/SiO_2 surfaces. In hexagonal mesophase at 102 °C (Figure 3, top), the characteristic 10 reflections (cf. Table 3) are observed at an angle of 60° with respect to each other. The intensity of the peak located on the meridian is significantly

Table 2. Diffraction Peaks Observed in the SAED Pattern of Figure 2 and Their Indexation to the α-Phase of PDPS

hkl	d_{exp} [Å]	d_{calc}[a] [Å]
200	9.60	9.58
400	4.78	4.79
600	3.18	3.19
800	2.38	2.39
101	4.72	4.83
211	4.23	4.32
301	3.88	3.93
002	2.43	2.50

[a] Key: here and in the following tables the *d*-spacings are calculated according to the data of ref 28.

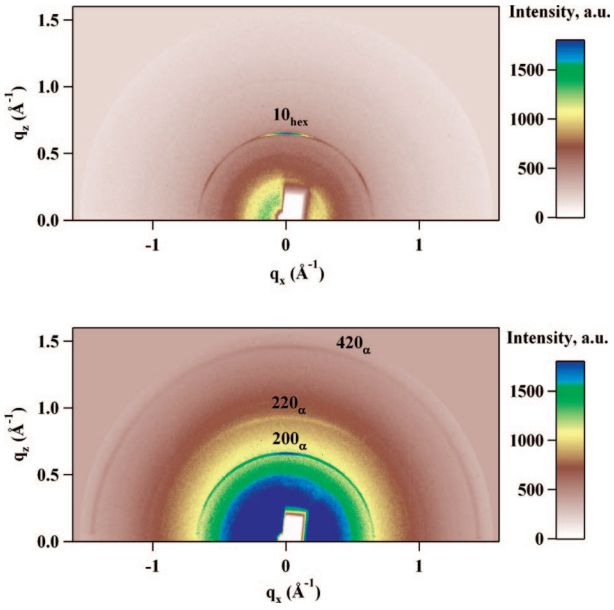

Figure 3. GIXD patterns of a fresh PDPS film spin-coated on a Si/SiO_2 substrate. Measurements are performed in the hexagonal mesophase at 102 °C (top) and in the crystalline phase at 28 °C (bottom).

Table 3. Diffraction Peaks Observed in GIXD Patterns of a Freshly Spin-Coated PDPS Film in the Mesophase at 102°C and in the α-Phase at 28 °C

α-phase			hexagonal mesophase		
hkl	d_{exp} [Å]	d_{calc} [Å]	*hkl*	d_{exp}[Å]	d_{calc} [Å]
200	9.56	9.58	10	9.70	9.68
220	6.79	6.77			
420	4.26	4.28			
211	4.31	4.32			

higher in comparison to the two other reflections. This can be explained by the presence of differently oriented mesomorphic domains obtained by rotation of the hexagonal lattice about the reciprocal space $\mathbf{10}_{hex}$ vector oriented normal to the substrate plane. Therefore, the film structure in the mesophase can be viewed as a layerlike arrangement of close-packed PDPS chains lying parallel to the substrate, with no preferential in-plane orientation. Upon crystallization of the sample, the intensity of the meridional peak remains strong (Figure 3, bottom). This reflection is assigned to the 200/020 peak of the α-crystal (cf. Table 2), which is in agreement with the zone axis of the SAED pattern given in Figure 2. The presence of this peak indicates that the layerlike arrangement of the PDPS chains is preserved after the phase transition from the mesophase to the α-crystal. However, no particular in-plane orientation can be detected in the crystalline film at room temperature.

To study the relations between the orientations of the mesomorphic and crystalline lattices of PDPS, the films with better orientation are needed. As mentioned above, the attempts to improve the film structure and orientation by annealing the films to different temperatures in the mesophase were unsuccessful. In the following, only the samples obtained after a short dwelling time above the isotropization temperature will be described.

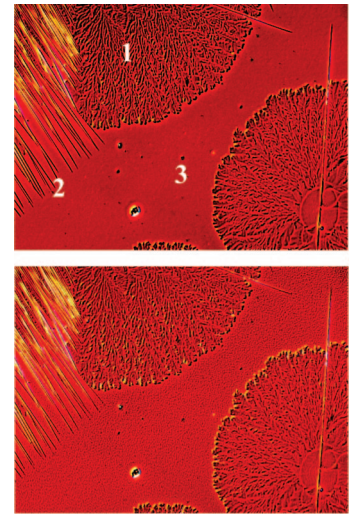

Figure 4. Top: optical micrograph showing the mesophase morphology in a thin film of PDPS at 200 °C. Two different morphological features are observed: cylindrites (1) and straight lamellar ribbons (2). Bottom: the same region after cooling down to room temperature, i.e., in the crystalline phase. The space not covered by the lamellar ribbons and cylindrites (3) acquires a grainy appearance due to crystallization. Image scale: 440 × 330 μm^2.

3.2. Morphology of the Spun-Cast Films of PDPS Annealed above the Isotropization Temperature. A short-term annealing of the spun-cast films above the isotropization temperature allows erasing the structural memory of the sample. Upon subsequent cooling of the film into the mesophase, one observes nucleation and growth of two distinct morphological features: circular objects, or cylindrites (N1 in the top panel of Figure 4) and long straight lamellar ribbons, or "needles", which can reach several hundreds of microns in length (N2 in the top panel of Figure 4). The growth of both types of entities continues until the full consumption of the amorphous material of the film. This process stops upon impingement of the cylindrites or needles on each other, implying that there is no transfer of material between the different mesomorphic entities. The mesophase growth can be also stopped by quenching the sample to a temperature below the melting point, e.g., to room temperature (Figure 4, bottom). In this case, the gross morphological features formed in the mesophase remain unchanged, whereas the previously featureless amorphous regions (N3 in the top panel of Figure 4) acquire a grainy appearance (Figure 4, bottom). Therefore, it is likely that the crystal growth proceeds in a different way in the regions with a mesophase structure already formed and in amorphous regions. The three distinct morphologies observed in thin films in the crystalline state, i.e., the grainy structure resulting from the quench-induced crystallization of the amorphous material, the lamellar ribbons, and cylindrites, will be separately described in the following.

A. PDPS Semicrystalline Morphology Obtained upon a Temperature Quench. AFM images recorded on a grainy region such as the one marked N3 in the top panel of Figure 4 reveal crystalline lamellae typical of many other semicrystalline polymers (Figure 5A). They are rather short (about 250 nm long) and do not exhibit any in-plane orientation. The power spectral density function (Figure 5B) exhibits a single broad interference maximum. The one-dimensional SAXS-type autocorrelation and

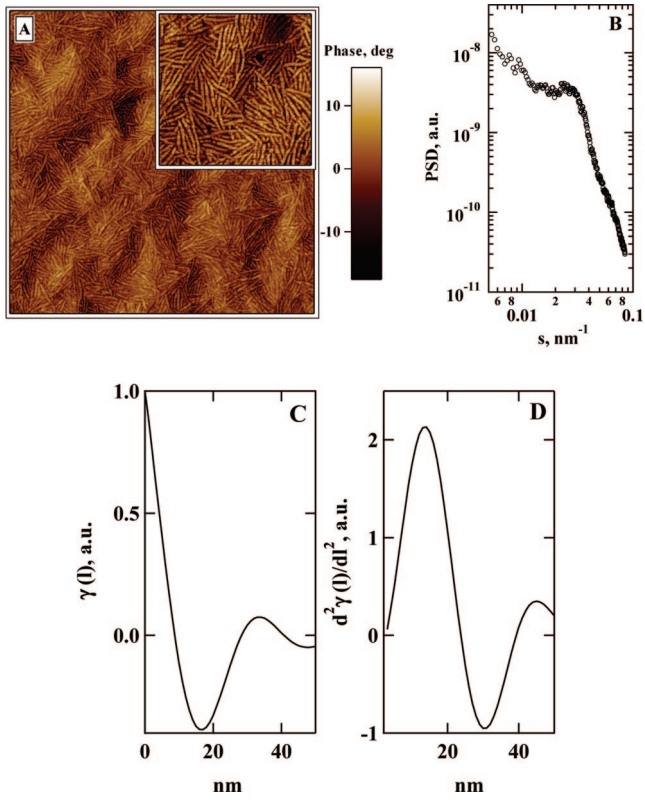

Figure 5. AFM Tapping Mode phase image (3.0 × 3.0 μm^2) of the PDPS crystallites formed by quenching the isotropic phase (A). The phase image in the inset (1.0 × 1.0 μm^2) gives a closer view of the semicrystalline lamellar morphology. The one-dimensional power spectral density function (B) and SAXS-type autocorrelation (C) and interface distribution (D) functions corresponding to the AFM image in A.

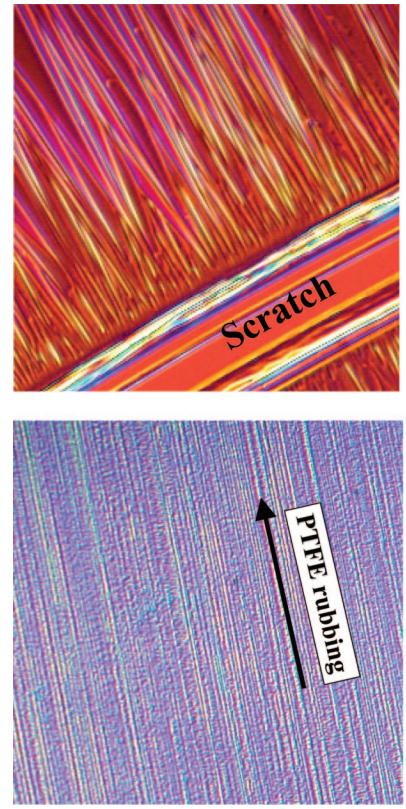

Figure 6. Top: OM image (150 × 150 μm^2) of a PDPS film spun-cast on a Si/SiO$_2$ substrate. The image shows the needles initiated by a scratch in the bottom right corner. Bottom: needles grown on a PTFE-rubbed surface; the rubbing direction is almost vertical. Image scale: 330 × 330 μm^2.

interface distribution functions corresponding to the AFM micrograph (Figure 5C,D) show that the long period of this structure is ~30 nm and crystal thickness is 15 nm. Therefore, the linear crystallinity in this region is only of 50%,[41] which is much lower than the overall crystallinity of PDPS crystallized from the mesomorphic state (e.g., 91% bulk crystallinty, as determined by X-ray diffraction[28]). A likely reason for such difference is that, in the absence of the mesophase structure, the PDPS crystallization occurs without significant lamellar thickening and therefore results in the conventional semicrystalline morphology for which the degree of crystallinity remains significantly below 100%. Apart from the lamellar structure, the micrograph shows bumps of larger size, which may correspond to the nascent spherulites that remain small due to a very high nucleation density.

B. Structure of the PDPS Lamellar Ribbons. In an attempt to prepare a macroscopically oriented sample by inducing directed growth of the mesophase, it was found that the mesomorphic ribbons can be generated by simply scratching the spun-cast film before the onset of the mesophase formation. In this case, bundles of oriented needles nucleate on the edges of the scratch and grow perpendicularly to the scratch direction, as shown in the top panel of Figure 6. This observation may infer that the ribbons are composed of the PDPS chains oriented parallel to the substrate and perpendicular to the ribbon axis. The quality of the alignment by scratch was found however insufficient for preparation of films uniformly oriented over several millimeters. Indeed, it can be seen that multiple structural defects appear during lamellar growth, for example due to collisions between the needles progressively deviating from their initial growth direction.

Another way to fabricate oriented mesomorphic films consists in the use of aligned substrates such as the surfaces of drawn PTFE initially proposed by Takahashi and coauthors[42] or PTFE-rubbed surfaces.[31,43] The alignment on such substrates of some semicrystalline polymers such as polyethylene, poly(ε-caprolactone), and nylon-6, with their chains spontaneously orienting parallel to the PTFE chain direction, was explained by the lattice matching. The PTFE-induced alignment of a main-chain LC polymer has not been reported to our knowledge yet. It is noteworthy that the PTFE-induced alignment of hexagonal columnar structures formed by small molecules (e.g., discotics) does not always show columnar orientation along the PTFE chain axis. Instead, the columns can have a tendency to orient homeotropically, whereby the columnar axes are perpendicular to the substrate plane.[44] This has been tentatively explained by the fluorophobic effect of the alkyl side chains that tend to minimize their contact with the substrate by adopting the homeotropic columnar orientation.

In this work, the PTFE-rubbed surfaces were found very efficient in aligning the mesomorphic PDPS up to the film thickness of about 2 μm. The PDPS needles in this case become oriented in the direction perpendicular to the PTFE rubbing. The bottom panel of Figure 6 shows an optical micrograph of a sample for which the PTFE rubbing direction is close to vertical. The needles are seen as small striations running perpendicular to the grooves formed during rubbing. They can be observed in more detail in AFM images of such a surface given in Figure 7, where the rubbing direction is almost horizontal. Accordingly, all the ribbons are oriented perpendicularly to the rubbing direction, i.e., vertically.

It is noteworthy that the PDPS morphology on the PTFE surface is entirely composed of the needles, which prompts us to think about the epitaxial mechanism of the mesophase

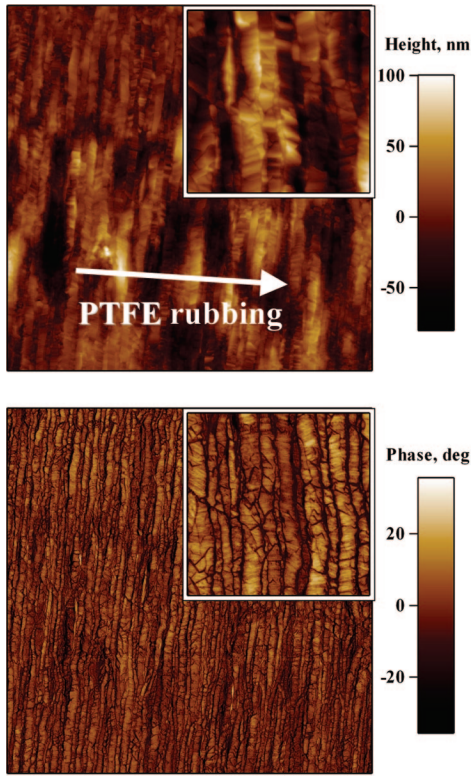

Figure 7. AFM Tapping Mode height (top) and phase (bottom) images ($10 \times 10\ \mu m^2$) measured at room temperature on the PDPS needles grown on a PTFE-rubbed surface. The PTFE rubbing direction is close to horizontal. The insets ($2.0 \times 2.0\ \mu m^2$) show the fine structure of the needles, which is explained by their crystalline state at room temperature.

formation. A closer examination of the oriented film morphology reveals that the needles have a variable width (Figure 7). This can be accounted for by the history of their local thickening process, which was interrupted at different moments by impingement of the neighboring needles. In addition, AFM images reveal a substructure of each needle consisting of stripes running at some angle to the needle axis. These features correspond to the facets of the crystals grown later from the mesomorphic needles and will be discussed in the following.

The films oriented by the PTFE-rubbed surface were studied by GIXD in the directions parallel and perpendicular to the rubbing (Figure 8); the observed reflections are summarized in Table 4. The diffraction patterns measured in the mesophase at ~100 °C exhibit hexagonal symmetry (Figure 8C). Despite the fact that notable intensity is spread along the arcs between diffraction peaks, intensities at the hexagonally positioned maxima are more or less equal, which is at variance with the previously discussed pattern of the as-spin-coated film (cf. Figure 3). In the perpendicular direction, only one meridional reflection is observed (Figure 8D), which confirms the hypothesis that the (*hk*) plane of the hexagonal lattice has a well-defined orientation perpendicular to the rubbing direction. Importantly, the hexagonal lattice of the needle adopts a unique orientation with the **10** reciprocal space vector pointing vertically. More quantitatively, the in-plane orientation of the mesomorphic needles was evaluated by performing GIXD scans as a function of angle ϕ, as depicted in the top panel of Figure 9. The bottom panel of the same figure shows the integral intensity of nonmeridional reflections of the hexagonal pattern corresponding to the PTFE rubbed layer and to the PDPS on PTFE. The PTFE layer exhibits a relatively sharp intensity distribution function with half-width at half-maximum (hwhm) of only 1.1°, which testifies its almost single-crystal-like structure. The doubling of the hexagonal PTFE lattice previously reported by Breiby and co-workers[45] has not been observed in our experiments. This can be due to a difference in the PTFE deposition conditions, which are known to strongly affect the deposited layer structure. Thus, in our case, the in-plane misalignment of the PTFE chains is somewhat higher as compared to the PTFE layers used in the work of Breiby. The alignment of PDPS along the rubbing direction, with hwhm of about 8.5°, reflects the epitaxial capacity of the PTFE layer. It is possible that the relatively broader angular distribution of the PDPS chains as compared to that of PTFE is brought about by depletion regions in the PTFE layer.

The resulting structure of the mesomorphic needles is schematically illustrated in Figure 10. Each mesomorphic column is depicted in the figure by a cylinder and corresponds to one individual PDPS chain. Comparing the width of the needles with the PDPS chain contour length, one can conclude that the chains in the needle are folded. The folding is expected to be most pronounced near the growing tip where the width of the needle is minimal.

To explain the lamellar orientation on the PTFE-rubbed surface, the lattice mismatch can be estimated based on the unit cell parameters and thermal dilatation coefficients of the hexagonal phase I of PTFE.[46] At the temperature of the PDPS mesophase growth (190 °C) the *a* parameter of PTFE is thus calculated to be 5.75 Å, which is about twice smaller than the lattice parameter of the PDPS mesophase (11.51 Å),[28] resulting in a perfect register between the two surfaces.

When such an oriented sample is cooled below its melting point, the hexagonal mesophase transforms into a crystal. In the GIXD patterns measured upon crystallization (Figure 8E,F), the characteristic six-spot pattern of the mesophase disappears to give rise to the peaks of the high-temperature α-crystalline form. The peaks indexation to the pseudotetragonal unit cell of the α-phase[28] allows identifying the presence of two different crystal orientations (Figure 11). The first one corresponds to the crystals having their **a** or **b** parameters oriented along the **a*** vector of the mesophase lattice. In this case, the lattice mismatch between the contact planes of the mesophase and crystal is virtually zero (cf. Figure 2 of ref 28). The growth of this crystal orientation is further favored by the fact that (100) and (010) planes are the fastest growing crystal faces, as was observed for the PDPS crystallization from dilute solutions.[30] The second crystal orientation corresponds to the crystals having the **110** direction parallel to the **a*** vector of the mesophase (Figure 11). The amount of such crystals is small, as can be seen from the relative intensities of the 200 and 220 peaks pertinent to both crystal orientations (Figure 8). This can be accounted for by a much bigger lattice mismatch (ca. 18% along the 110 plane), which should be prohibitive for efficient epitaxial crystallization. It is also possible that the crystal growth starts in this case directly from the PTFE surface, with which the lattice mismatch is comparable.

C. Structure of the PDPS Cylindrites. The predominantly cylindritic morphology was generated in PDPS films upon a long-time annealing at a high temperature. It was found rather difficult to completely exclude the presence of the needles. However, by varying the mesophase formation temperature, it was possible to strongly limit their amount and to obtain large surface regions composed only of the cylindrites. Figure 12 displays typical SAED patterns measured on such films at room temperature. The top pattern was recorded using a short exposure (2 s), which was started immediately after beginning of observation. The pattern reveals the characteristic pseudotetragonal symmetry of the α-phase, which means that in the cylindrites the PDPS chains are vertical with respect to the substrate plane. The in-plane lattice orientation was studied by examining the sample in diffraction mode. Within each cylin-

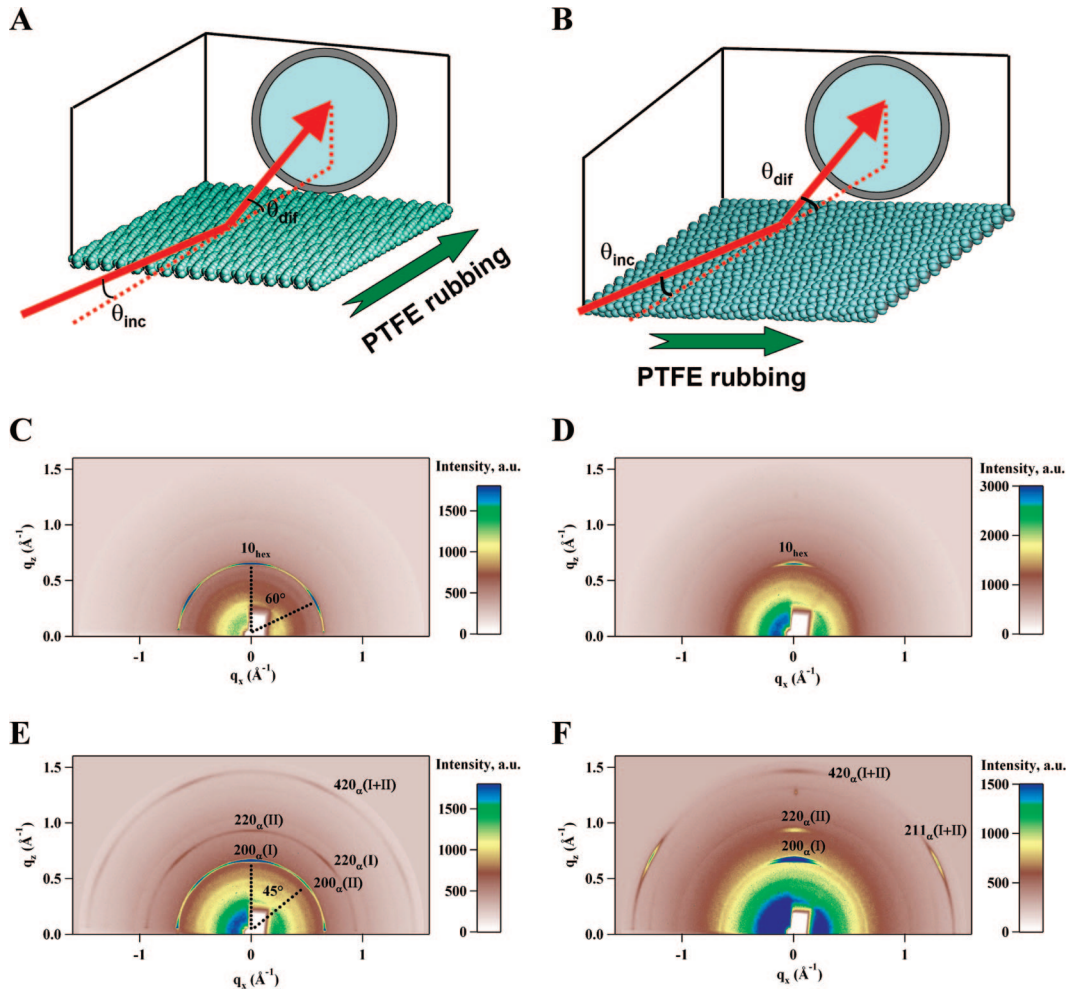

Figure 8. GIXD patterns of a PDPS thin film on a PTFE-rubbed surface measured after annealing. The X-ray beam is directed parallel (A, C, E) or perpendicular (B, D, F) to the rubbing direction. The measurements are performed in the mesophase at 102 °C (C, D) and in the crystalline phase at 28 °C (E, F).

Table 4. Diffraction Peaks Observed in GIXD Patterns of Annealed Films Deposited on PTFE-Rubbed Surfaces (cf. Figure 8)

α			hexagonal mesophase		
hkl	d_{exp} [Å]	d_{calc} [Å]	*hkl*	d_{exp}[Å]	d_{calc} [Å]
200	9.48	9.58	10	9.67	9.68
220	6.74	6.77			
400	4.75	4.79			
420	4.25	4.28			
440	3.40	3.39			
101	4.81	4.83			
211	4.28	4.32			
301	3.91	3.93			
321	3.59	3.64			
411	3.38	3.40			

drite, the lattice orientation was found to be largely invariable. Only a slight variation of the relative peak intensities with the beam position was sometimes detected, which could indicate on some imperfections in the homeotropic chain orientation.

The structure of the sample was however dramatically changing after longer exposure times (Figure 12, bottom). Thus, after about 3 s of the sample exposure in the beam, one can see the appearance of additional diffraction peaks, which can be assigned to the PDPS hexagonal mesophase. The observed transformation of the α-phase to the mesophase is therefore caused by the electron beam. Importantly, the orientation of the mesophase with respect to that of the parent crystalline phase is well-defined: the reciprocal space **a*** vector of the mesophase is parallel to the **a** or **b** vectors of the α-crystal. This is similar to what was observed for crystallization of the needles in crystal orientation I (cf. Figure 11, left) and can be accordingly explained by the epitaxial nucleation of the mesophase on the crystalline phase. Previously, the crystal-to-mesophase transformation under the electron beam was reported for single crystals of PDPS.[30]

Further studies of the cylindrite structure were performed with GIXD using the PDPS sample of 269 000 g/mol. In the mesophase, the 10 peak is visible only along the equatorial direction (Figure 13, top), meaning that the previously described signature of the needles is not present in the pattern. The conclusions about the homeotropic chain alignment in the cylindrites drawn from the electron diffraction experiments are thus confirmed. The structure of the mesomorphic cylindrites is schematically depicted in Figure 14.

The room temperature GIXD pattern corresponding to the cylindrites in the α-crystalline form is given in the bottom panel of Figure 13. In this case, a broad off-meridional 101 peak appears along the vertical direction, while the 200 and 220 reflections are visible on the equator. This demonstrates that the vertical chain orientation is preserved upon crystallization. Importantly, in contrast to the PDPS fiber pattern[28] the relative intensity of the 220 peak is much weaker than that of the 200 peak. This can be accounted for by the microstructure of the film composed of large cylindrites having a single-crystal-like nature. The uniaxial symmetry, typical of the fiber structure, is

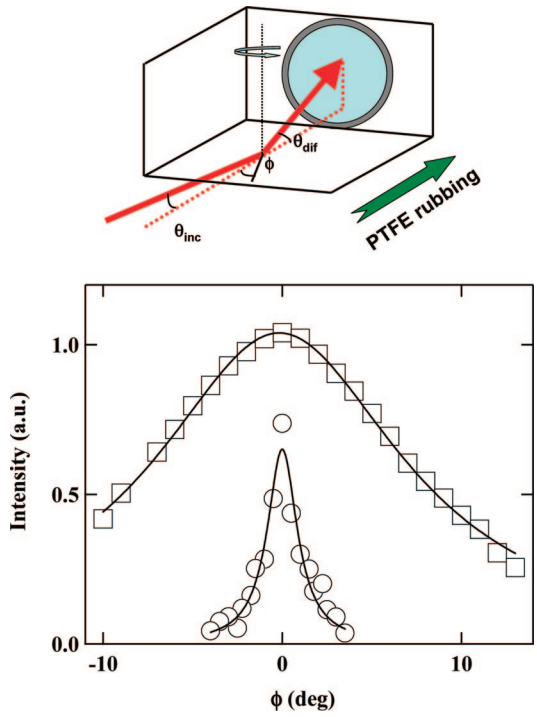

Figure 9. Determination of the in-plane orientation using GIXD scans as a function of angle ϕ (top). Angular variation of the integral intensity of nonmeridional peaks of the hexagonal lattices of PTFE (circles) and PDPS on PTFE (squares) recorded at 102 °C (bottom). The lines are guides for the eye.

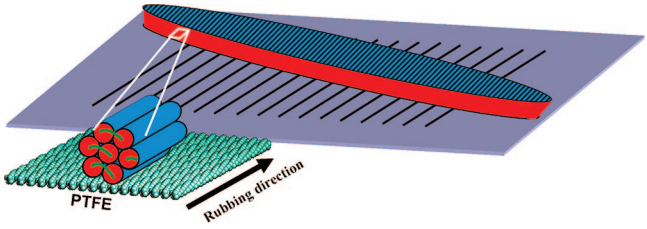

Figure 10. Schematic representation of the microstructure of the mesomorphic lamellar ribbons of PDPS. Each cylinder corresponds to one individual PDPS chain, the axes of which are arranged on a hexagonal 2D lattice. For the sake of clarity, the polar backbones, apolar side chains, and chain folds are given in red, blue, and green, respectively. The PDPS chain axes are aligned along the rubbing direction of PTFE.

probably lost, and the reflection conditions for some of the equatorial peaks are not satisfied.

3.3. General Discussion on the Mesomorphic and Crystalline Film Morphology. The main result stemming from the study of the mesomorphic PDPS film structure is that only two discrete chain orientations are detected in the films. In the lamellar ribbons, the PDPS backbones are lying in the plane of the film. By contrast, in the cylindrites the chains stand vertically. From the morphological point of view, both entities, i.e., the cylindrites and needles, are in fact the same lamellae that develop differently because of the geometrical confinement imposed by the film. Indeed, the needles can be viewed as the PDPS lamellae having their basal planes, or fold surfaces, normal to the substrate (cf. Figure 10), whereas in the cylindrites they are oriented parallel to the film surface (cf. Figure 14). In bulk, both entities would be indistinguishable because, for example, the needles could continue their lateral growth vertically and the cylindrites would be able to thicken along the same direction. Although in the thin films studied both entities coexist, the impact of confinement on the thermodynamics should be more dramatic for the case of the cylindrites, the growth of which is limited by the fold planes. For the needles, this effect is expected to be weaker because their limiting planes are parallel to the chain axes that, in analogy with the semicrystalline state, will require smaller free energy expenditure.

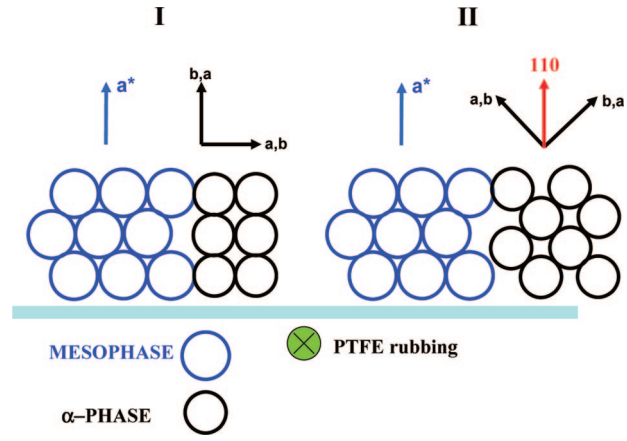

Figure 11. Epitaxial relationships between the "parent" hexagonal mesophase and the growing α-crystal of PDPS. Two different crystal orientations result from such mesophase-assisted crystallization: in orientation I the **a** or **b** vectors are vertical; in orientation II the **110** vector is vertical.

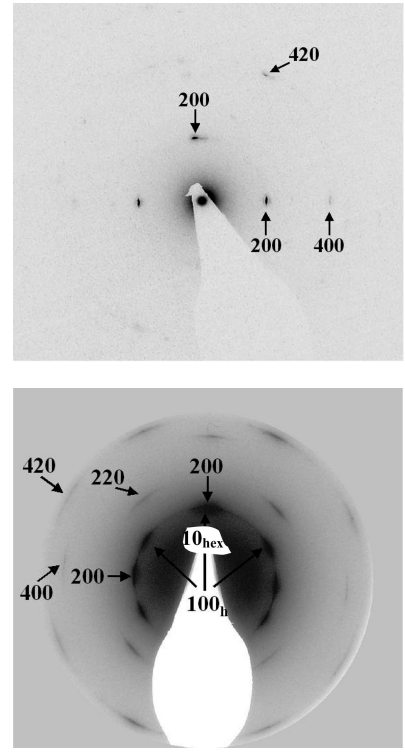

Figure 12. Top: SAED pattern corresponding to a cylindrite in the crystalline α-phase recorded during a short exposure time at the very beginning of observation. Bottom: SAED pattern recorded on a similar region after longer observation. The pattern exhibits the diffraction peaks pertinent to both the crystalline α-phase and hexagonal mesophase (10_{hex}).

Importantly, for both, the needles and cylindrites, the chain axes are perpendicular to the basal lamellar planes.[47] This can account for the observation of only two chain orientations in the films. Obviously, the mesomorphic entities having a different chain orientation would not be able to reach large lateral dimensions without being limited by the film interfaces.

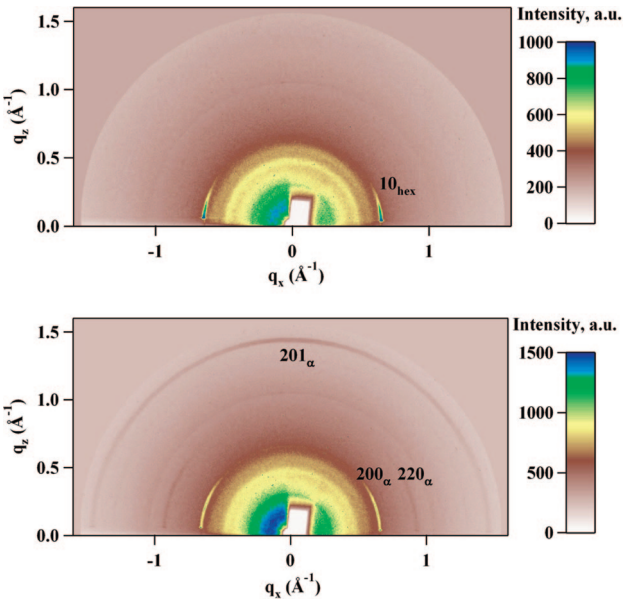

Figure 13. GIXD patterns of an annealed PDPS thin film on a bare silicon wafer recorded at 102 °C (top) and 28 °C (bottom).

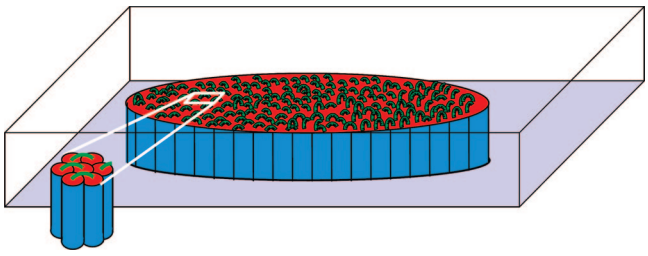

Figure 14. Schematic representation of the microstructure of the mesomorphic cylindrites of PDPS. See the legend in the caption of Figure 10.

Alternatively, to grow laterally, the PDPS chains in the lamellae would need to adopt a tilt with respect to the basal plane normal, the situation which was not observed in the experiments.

The process of the PDPS thin film crystallization leaves the large-scale morphological features formed during the mesophase growth largely unaffected. This is at variance with what is known for the polymer crystallization from the isotropic melt and therefore shows the importance of the chain preordering in the mesophase. The classical semicrystalline lamellar morphology of PDPS can be formed only in the amorphous regions remaining after quenching the sample from a high temperature such as those marked with N3 in Figure 4. In the mesomorphic regions, the process of crystallization is guided by the mesophase orientation and structure. Thus, the dominating crystal orientation, i.e., orientation I in Figure 11, results from the epitaxial nucleation and growth of crystalline α-phase on the parent mesophase. The structural similarity between the mesophase and crystal can explain the high crystallization rates observed in the experiments. Contrary to crystallization from the isotropic melt, the mesophase-assisted crystallization does not involve the time-consuming process of reeling the chain from the melt onto the growing crystal surface with chain folding. Instead, the crystallization operates essentially on the submolecular scale by adjusting the conformations of the already disentangled and preordered backbones, which allows to dramatically accelerating its kinetics. The resulting crystalline state is characterized by the practical absence of amorphous regions and, consequently, a very high degree of crystallinity that cannot be achieved after "normal" polymer crystallization from the isotropic melt.

4. Conclusions

The structure formation and phase transitions in thin PDPS films were studied with a combination of optical and atomic force microscopy as well as with electron diffraction and grazing incidence X-ray diffraction. Two different morphological features are observed in the mesomorphic PDPS films. The lamellar ribbons, or needles, are composed of the chains oriented parallel to the plane of the substrate in such a way that the reciprocal space **10** vector of the mesophase lattice is vertical. The other morphological feature having a circular symmetry, the cylindrite, contains the chains parallel to the substrate normal. For both morphological entities the lattice orientation is preserved over macroscopic distances, as shown with SAED and GIXD.

The cylindrites and needles are essentially the same mesomorphic lamellae having a structure similar to that of the bulk polymer but that develop differently under the conditions of geometrical confinement. The difference between the two features thus exists only in thin films. The chain axes in both features are normal to the basal, or fold, plane, which explains why the mesomorphic PDPS films exhibit only these two discrete chain orientations.

The crystallization of PDPS films does not change the gross morphological features developed during the mesophase growth because the crystallization process mainly operates on the submolecular scale. In the resulting structure, the dominant population of crystals having **a** or **b** vectors oriented along the **a*** vector of the mesophase lattice is formed. This is explained by the epitaxial nucleation and growth of the α-crystal on the parent mesophase, with a perfect register between the contact planes of the two phases.

It was found that thin films of mesomorphic PDPS can be spontaneously aligned on the PTFE-rubbed surface, which is accounted for by the surface epitaxy. In this case, the PDPS chains are oriented parallel to the PTFE chain direction, which is a usual observation for such substrates. Subsequent crystallization of PDPS fixes the film microstructure giving rise to a macroscopically oriented highly crystalline polymer surface.

Acknowledgment. The authors are grateful to B. Lotz, G. Ungar, and A. N. Semenov for helpful discussions and to M. Rosenthal for the design of a computer code allowing for the X-ray data reduction and treatment. GIXD measurements were carried out at the National Synchrotron Light Source, Brookhaven National Laboratory, which is supported by the U.S. Department of Energy, Division of Materials Sciences and Division of Chemical Sciences, under Contract DE-AC02-98CH10886. M.D. gratefully acknowledges financial support from the CNRS and Region of Alsace (BDI bursary).

References and Notes

(1) Pyrasch, M.; Toutianoush, A.; Jin, W.; Schnepf, J.; Tieke, B. *Chem. Mater.* **2003**, *15*, 245.
(2) Bearzotti, A.; Bertolo, J. M.; Innocenzi, P.; Falcaro, P.; Traversa, E. *J. Eur. Ceram. Soc.* **2004**, *24*, 1969.
(3) Tang, C. W.; VanSlyke, S. A. *Appl. Phys. Lett.* **1987**, *51*, 913.
(4) Schmidt-Mende, L.; Fechtenkötter, A.; Müllen, K.; Moons, E.; Friend, R. H.; MacKenzie, J. D. *Science* **2001**, *293*, 1119.
(5) Dimitrakopoulos, C. D.; Malenfant, P. R. L. *Adv. Mater.* **2001**, *14*, 99.
(6) Sirringhaus, H.; et al. *Nature (London)* **1999**, *401*, 685.
(7) Loo, Y.-L.; Register, R. A. *Macromolecules* **2002**, *35*, 2365.
(8) Zhu, L.; Cheng, S. Z. D.; Calhoun, Bret, H.; Ge, Q.; Quirk, R. P.; Thomas, E. L.; Hsiao, B. S.; Yeh, F.; Lotz, B. *J. Am. Chem. Soc.* **2000**, *122*, 5957.
(9) Zhu, L.; Cheng, S. Z. D.; Calhouna, B. H.; Gea, Q.; Quirk, R. P.; Thomas, E. L.; Hsiao, B. S.; Yeh, F.; Lotz, B. *Polymer* **2001**, *42*, 5829.
(10) Shibaev, V. P.; Platé, N. A. *Adv. Polym. Sci.* **1984**, *60*, 175.
(11) Finkelmann, H.; Rehage, G. *Adv. Polym. Sci.* **1984**, *60*, 100.
(12) Ungar, G. *Polymer* **1993**, *34*, 10.

(13) Busch, P.; Krishnan, S.; Paik, M.; Toombes, G. E. S.; Smilgies, D.-M.; Gruner, S. M.; Ober, C. K. *Macromolecules* **2007**, *40*, 81.
(14) Al-Hussein, M.; Séréro, Y.; Konovalov, O.; Mourran, A.; Möller, M.; de Jeu, W. H. *Macromolecules* **2005**, *38*, 9610.
(15) Hikosaka, M.; Rastogi, S.; Keller, A.; Kawabata, H. *J. Macromol. Sci., Part B* **1992**, *31*, 87.
(16) Beatty, C. L.; Pochan, J. M.; Froix, M. F.; Hinman, D. D. *Macromolecules* **1975**, *8*, 547.
(17) Godovsky, Yu., K.; Papkov, V. S. *Adv. Polym. Sci.* **1989**, *88*, 129.
(18) Molenberg, A.; Möller, M.; Sautter, E. *Prog. Polym. Sci.* **1997**, *22*, 1133.
(19) Godovsky, Yu., K.; Papkov, V. S. *Makromol. Chem., Macromol. Symp.* **1986**, *4*, 71.
(20) Godovsky, Yu., K.; Makarova, N. N. *Philos. Trans. R. Soc. London A* **1994**, *>348*, 45.
(21) Molenberg, A.; Möller, M. *Macromolecules* **1997**, *30*, 8332.
(22) Molenberg, A. Ph.D. Thesis, University of Ulm, Germany, **1997**.
(23) Godovsky, Yu. K.; Mamaeva, I. I.; Makarova, N. N.; Papkov, V. S.; Kuzmin, N. N. *Makromol. Chem., Rapid Commun.* **1985**, *6*, 797.
(24) Out, G.; Turetskii, A. A.; Möller, M.; Oelfin, D. *Macromolecules* **1994**, *27*, 3310.
(25) Slottke, H. Die Konformation der mesophasenbildender Poly(di-n-alkylsiloxane). Ph.D. Thesis, University of Mainz, Germany, **1995**.
(26) Out, G.; Turetskii, A. A.; Möller, M. *Macromol. Rapid Commun.* **1995**, *16*, 107.
(27) Godovsky, Yu., K.; Makarova, N. N.; Papkov, V. S.; Kuzmin, N. N. *Makromol. Chem., Rapid Commun.* **1985**, *6*, 443.
(28) Gearba, R. I.; Anokhin, D. V.; Bondar, A. I.; Godovsky, Yu, K.; Papkov, V. S.; Makarova, N. N.; Magonov, S. N.; Bras, W.; Koch, M. H. J.; Masin, F.; Goderis, B.; Ivanov, D. A. *Macromolecules* **2006**, *39*, 988.
(29) Shulgin, A. I.; Godovsky, Yu, K.; Makarova, N. N. *Thermochim. Acta* **1994**, *238*, 337.
(30) Gearba, R. I.; Dubreuil, N.; Anokhin, D. V.; Godovsky, Yu, K.; Ruan, J.-J.; Thierry, A.; Lotz, B.; Ivanov, D. A. *Macromolecules* **2006**, *39*, 978.
(31) Wittmann, J. C.; Smith, P. *Nature (London)* **1991**, *352*, 414.
(32) Barna, S. L.; Tate, M. W.; Gruner, S. M.; Eikenberry, E. F. *Rev. Sci. Instrum.* **1999**, *70*, 2927.
(33) Godovsky, Y. K.; Papkov, V. S.; Magonov, S. N. *Macromolecules* **2001**, *34*, 976.
(34) Magonov, S. N. Atomic Force Microscopy in Analysis of Polymers. In *Encyclopedia of Analytical Chemistry*; Meyers, R. A., Ed.; John Wiley & Sons Ltd.: Chichester, England, 2000; p 7432.
(35) Basire, C.; Ivanov, D. A. *Phys. Rev. Lett.* **2000**, *85*, 5587.
(36) Ivanov, D. A.; Amalou, Z.; Magonov, S. N. *Macromolecules* **2001**, *34*, 8944.
(37) Press, W. H.; et al. *Numerical Recipes in C, The Art of Scientific Computing*; Plenum Press: New York, 1988.
(38) Ruland, W. *Colloid Polym. Sci.* **1977**, *255*, 417.
(39) Koberstein, J. T.; Morra, B.; Stein, R. S. *J. Appl. Crystallogr.* **1980**, *13*, 34.
(40) Balta-Calleja F. J.; Vonk, C. G. *X-ray Scattering of Synthetic Polymers*; Elsevier: Amsterdam, 1989.
(41) In the analyzed AFM image, most of the lamellar crystals are close to the edge-on orientation, which makes the calculation of the 1D correlation and interface distribution functions meaningful. Importantly, a small tilt of the lamellar planes with respect to the substrate normal will not affect the computed linear crystallinity values.
(42) Takahashi, T.; Teraoka, F.; Tsujimoto, I. *J. Macromol. Sci., Phys.* **1976**, *B12*, 303.
(43) Wittman, J. C.; Lotz, B. *Prog. Polym. Sci.* **1990**, *15*, 909.
(44) Gearba, R. I.; Anokhin, D. V.; Bondar, A. I.; Bras, W.; Lehmann, M.; Ivanov, D. A. *Adv. Mater.* **2007**, *19*, 815.
(45) Breiby, D. W.; Sølling, T. I.; Bunk, O.; Nyberg, R. B.; Norrman, K.; Nielsen, M. M. *Macromolecules* **2005**, *38*, 2383.
(46) Clark, E. S. *J. Macromol. Sci., Part B: Phys.* **2006**, *45*, 201.
(47) In this consideration, the slight chain tilt resulting from the tapered shape of the lamellar tip such as described by Keller and co-authors (cf. ref 15) is neglected.

MA802666A